Michigan State University

National Superconducting Cyclotron Laboratory

SOURCES AND EMISSION TIME SCALES IN E/A = 50 MeV $^{129}Xe + ^{nat}Cu$ REACTIONS

D.R. BOWMAN, G.F. PEASLEE, N. CARLIN, R.T. de SOUZA, C.K. GELBKE, W.G. GONG, Y.D. KIM, M.A. LISA, W.G. LYNCH, L. PHAIR, M.B. TSANG, C. WILLIAMS, N. COLONNA, K. HANOLD, M.A. McMAHAN, G.J. WOZNIAK, and L.G. MORETTO

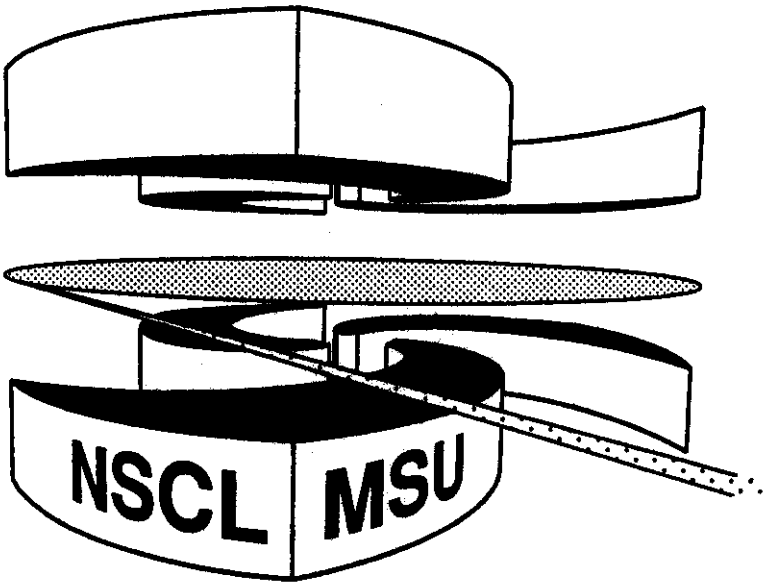

MSUCL-862 **DECEMBER 1992**

MSUCL-862
December, 1992

Sources and Emission Time Scales in E/A = 50 MeV ^{129}Xe + ^{nat}Cu Reactions

D.R. Bowman*, G.F. Peaslee, N. Carlin†, R.T. de Souza‡, C.K. Gelbke, W.G. Gong§, Y.D. Kim**, M.A. Lisa, W.G. Lynch, L. Phair, M.B. Tsang, and C. Williams

National *Superconducting Cyclotron Laboratory and Department of Physics and Astronomy, Michigan State* University, *East Lansing, MI 48824*

N. Colonna††, K. Hanold, M.A. McMahan, G.J. Wozniak, and L.G. Moretto

Nuclear Science Division *and Accelerator and Fusion Research* Division, Lawrence *Berkeley Laboratory, Berkeley, CA 94720*

Distributions in velocity space and fragment-fragment correlation functions have been measured as a function of the charged particle multiplicity for ^{129}Xe t ^{nat}Cu collisions at E/A=50 MeV. With increasing multiplicity, the velocity distributions evolve from a two-component pattern to an anisotropic distribution with no discernable source. The corresponding correlation functions indicate fragment emissions times consistent with a two source mechanism for low multiplicity collisions; but the time scale for fragment emission in the high multiplicity collisions is too short for a separation of sources to occur.

Recent experiments have demonstrated that nuclear systems undergo a multifragment disassembly following heavy ion reactions at both high [1–5] and intermediate bombarding energies [6–14]. The breakup mechanism has been associated with volume instabilities [15, 16], which are related to a liquid-gas phase transition in nuclear matter [17]; with a series of statistical binary decays [18–21]; or with surface instabilities which can arise if nuclear systems attain exotic shapes [22, 23]. While the theoretical description of the multifragmentation process remains a matter of contention, two experimental methods have been used to characterize the sources of fragment emission: the analysis of kinematic distributions, and the extraction of emission time scales via fragment-fragment correlation functions.

The observation of "Coulomb circles" in the fragment velocity distributions has been used to demonstrate the binary nature of reactions with asymmetric entrace channels [18], and been interpreted as evidence for an underlying binary character in reactions with more symmetric entrance channels [12]. However, taken by themselves, velocity plots give no quantitative information on the time scale of fragment emission and can lead to contradictory interpretations [24, 25]. Fragment-fragment correlation functions are able to provide such information [26–29]. In this paper, for the first time, we obtain a consistent picture of peripheral and central collisions by simultaneously measuring the fragment distributions in velocity space and fragment-fragment correlation functions for two charged particle multiplicity gates.

The experiment was performed using the K1200 Cyclotron at the National Superconducting Cyclotron Laboratory at Michigan State University. A beam of ^{129}Xe ions with intensity $\sim 10^7$ particles/s impinged upon ^{nat}Cu targets of thickness 2 mg/cm^2. Intermediate mass fragments and light charged particles were detected at angles of 16°-160° using the MSU Miniball phoswich array [30], which covered approximately 87% of 4π. At more forward angles, 2°-16°, 16 position-sensitive Si-Si(Li)-Plastic

telescopes were placed [31]. The energy calibrations are estimated to be accurate to 1% for fragments stopped in the Si(Li) detectors and 5-10% for fragments and particles detected with the Miniball. The position resolution of the Si telescopes is approximately ± 1.5 mm in both the X and Y dimensions. Additional experimental details are given in Ref. [14].

Figure 1 shows the cross sections in velocity space for Z=2 and Z=6 fragments with two different gates on the total charged particle multiplicity, N_C. The limits of the detector acceptance are indicated by the solid lines in the figure. In order to obtain continuous distributions, the yields at angles $>16°$ have been randomized over the face of the struck Miniball detector.

Peripheral collisions (left hand panels) show two well separated components. One component is centered at a parallel velocity slightly less than that of the beam (indicated by the black arrows in the left hand panels) and the other is centered at a parallel velocity slightly larger than zero. We interpret these components as due to the decay of projectile-like (PLF) and target-like fragments (TLF). The shape of these distributions is similar to that expected for emission from two well-defined sources. However, these sources cannot be completely equilibrated since the emission is preferentially backward in the frame of the PLF, and preferentially forward in the frame of the TLF.

The right hand panels in Figure 1 show similar distributions in velocity space for Z=2 and Z=6 fragments gated on high multiplicity collisions. Under these conditions we observe broad, anisotropic distributions centered approximately near the center-of-mass velocity (black arrows on the right-hand panels), but with no clearly distinguishable source.

In order to obtain quantitative information about the time scales of fragment emission we have constructed two-fragment, velocity correlation functions defined as:

$$\sum Y_{12}(\mathbf{v_1}, \mathbf{v_2}) = C[1 + R(v_{red})] \sum Y_1(\mathbf{v_1}) Y_2(\mathbf{v_2}),$$

where $\mathbf{v_1}$ and $\mathbf{v_2}$ are the laboratory velocities of the fragments, v_{red} is the reduced relative velocity, $v_{red} = (\mathbf{v_1} - \mathbf{v_2})/(Z_1 + Z_2)$, and C is a normalization constant determined by requiring $R(v_{red}) \approx 0$ at large relative velocities where the final state interaction is small. The singles yields, Y_1 and Y_2 are taken from the same events as the coincidence yields, Y_{12}. The reduced relative velocity, v_{red}, is introduced to eliminate the charge dependence of the relative fragment velocity in mixed fragment correlation functions [28, 32]. We have verified with $Z_1 = Z_2$ correlation functions that there is little dependence of v_{red} on Z for v_{red} >0.01c.

In Figure 2 we show mixed fragment correlation functions ($5 \leq Z_1, Z_2 \leq 12$) for fragments stopped in the Si(Li) detectors. Although limited to fragment pairs with $2° < \theta_1, \theta_2 < 16°$, the acceptance in the center-of-mass (CM) system is quite reasonable due to the reverse kinematics employed in this experiment. In the top panel correlation functions gated on high multiplicity are presented for three gates on the CM velocity of the two fragments. In the bottom panel are the correspondingly gated correlation functions for low multiplicity collisions. While there are quantitative differences in the high multiplicity correlation functions for different values of CM velocity, the shapes of the curves are similar. This relative independence on the CM velocity can be contrasted with the correlation functions gated on low multiplicity, where there is a dramatic difference in shape.

Let us consider the peripheral reactions first. In order to quantify the fragment emission time scale, we have performed 3-body trajectory simulations [27, 28, 32]. Because a combination of sources can give rise to correlation functions which cannot be easily interpreted [33], we have chosen to select fragment pairs from low-multiplicity collisions with a CM velocity >0.3c. This cut suppresses contributions from the

target-like source (see Fig. 1). Simulated events were generated using the experimental charge, energy, and angular distributions; subsequently filtered through a software replica of the experimental apparatus; and analyzed in the same manner as the experimental data.

The calculated correlation functions are sensitive to the space-time extent of the emitting source. In the simulations we have fixed the source radius, R_S, at 10 fm and the total charge, mass, and velocity of the system at 54, 129, and 0.33c, respectively, equal to the projectile charge, mass and velocity. In the bottom panel of Fig. 3, the simulated correlation function with mean emission times, τ, of 100, 200, and 500 fm/c are compared with the experimental data; a mean emission time of 200 fm/c gives the best agreement with the data [34]. We have performed other calculations with identical emission times and R_S=8 and 12 fm [35]. To quantify the agreement between the simulations and the experimental data, the reduced χ^2 values for the simulations are presented in Table 1 [36]. For any reasonable choice of radius parameter, the time scale for emission of high velocity fragments in peripheral reactions is on the order of 200 - 500 fm/c.

Now let us consider the central reactions. We have placed no gate on CM velocity due to a lack of distinct sources and the similarity of the velocity gated correlation functions shown in the upper panel of figure 2. For these simulations we have chosen a source charge, mass, and velocity of 83, 193, and 0.22, respectively, corresponding to complete fusion of projectile and target. In the top panel of Fig. 3 the experimental data for high multiplicity collisions are compared with 3-body trajectory calculations with R_S=12 fm and τ=0, 50, 100, and 200 fm/c. The data show best agreement with the simulation for τ=100 fm/c. In Table 2, the reduced χ^2 values for these simulations, along with others with identical mean emission times and R_S=10 and 14 fm [35] are shown [36]. For any reasonable choice of radius parameter, the time

scale for fragment emission in central collisions is $\leq$100 fm/c. These time scales are consistent with those extracted for central collisions in ^{36}Ar + ^{197}Au reactions at E/A = 35 - 110 MeV [27–29].

The observed distributions of fragments in velocity space (Fig. 1) indicate emission time scales for peripheral collisions long enough to allow a separation of the PLF and the TLF, as predicted by the deep inelastic scattering and incomplete fusion mechanisms, but shorter than the rotational times of the excited PLF and TLF. Assuming a relative velocity equal to the beam velocity, the time required for the ^{129}Xe projectile to pass the ^{nat}Cu target is $\approx$70 fm/c. This time can be taken as a lower limit to the projectile-target separation time; any dissipation of the entrance channel kinetic energy will give a longer separation time. The time necessary for rotation of a ^{129}Xe nucleus with angular momentum of J=88$\hbar$ [37] is approximately 700 fm/c (smaller values of J will lead to correspondingly longer rotational times). As expected, the emission time of 200-500 fm/c extracted for high velocity fragments in peripheral collsions falls between the PLF-TLF separation time and the PLF rotational time.

The emission time scale of of $\leq$100 fm/c extracted for central collisions is similar to the separation time of the PLF and TLF calculated above. This short time scale precludes PLF/TLF mechanisms such as deep inelastic scattering or incomplete fusion and accounts for the lack of discernable sources in the observed velocity distributions.

We have investigated the uncertainties in the results of the 3-body simulations by varying the source velocity and source charge. The source velocity was varied between the nucleon-nucleon CM velocity (0.16c) and the beam velocity (0.33c). The source charge was varied between 0 and 83 (complete fusion). In the region of v_{red} <0.02c the uncertainties due to source velocity and source charge correspond to an uncertainty in mean emission time of $\approx$50 fm/c.

In summary, we have simultaneously measured fragment distributions in velocity

space and fragment-fragment velocity correlation functions for $^{129}Xe + {}^{nat}Cu$ reaction at E/A=50 MeV. A consistent picture emerges for both peripheral and central collisions. Peripheral collisions are characterized by two sources which decay on a time scale long enough to allow their separation in space, but of insufficient lifetime to allow complete equilibration. Central collisions are characterized by broad anisotopic distribution in velocity space and a fast time scale insufficient to allow even a separararation of sources.

Fruitful discussions with Scott Pratt are gratefully acknowledged. This work was supported by the National Science Foundation under Grant PHY-89-13815 and the U.S. Department of Energy under Contract No. DE-AC03-76SF00098. W.G.L acknowledges support from the U.S. Presidential Young Investigator Program and N.C. acknowledges partial support by the FAPESP, Brazil.

REFERENCES

* Present Address: Chalk River Laboratories, Chalk River, Ontario K0J 1J0, Canada.

† Present Address: Instituto de Fisica, Universidade de Sao Paulo, C. Postal 20516, CEP 01498, Sao Paulo, Brazil.

‡ Present Address: Department of Chemistry and Indiana University Cyclotron Facility, Bloomington, IN 47405.

§ Present Address: Lawrence Berkeley Laboratory, Berkeley, CA 94720.

** Present Address: Indiana University Cyclotron Facility, Bloomington, IN 47405.

†† Present Address: INFN - Sez. di Bari, 70126 Bari, Italy.

[1] J.W. Harris et al., Nucl. Phys. **A471**, 241c (1987).

[2] C.A. Ogilvie et al., Phys. Rev. Lett **67**, 1214 (1991).

[3] J. Hubele et al., Z. Phys. **A340**, 263, (1991).

[4] J.P. Alard et al., Phys. Rev. Lett. **69**, 889 (1992).

[5] J. Hubele et al., Phys. Rev. **C46**, R1577 (1992).

[6] Y.D. Kim et al., Phys. Rev. Lett. **63**, 494 (1989).

[7] Y. Blumenfeld et al., Phys. Rev. Lett. **66**, 576 (1991).

[8] E. Piasecki et al., Phys. Rev. Lett. **66** 1291 (1991).

[9] D.R. Bowman et al., Phys. Rev. Lett. **67** 1527 (1991).

[10] R.T. de Souza et al., Phys. Lett. **B268** 6 (1991).

[11] K. Hagel et al., Phys. Rev. Lett. **68** 2141 (1992).

[12] B. Lott et al., Phys. Rev. Lett. **68** 3141 (1992).

[13] T.C. Sangster et al., Phys. Rev. **C46**, 1404 (1992).

[14] D.R. Bowman et al., Phys. Rev. **C46**, 1834 (1992).

[15] J.P. Bondorf et al., Nucl. Phys. **A443** 321 (1985); ibid **444** 460 (1985).

[16] D.H.E. Gross et al., Phys. Rev. Lett. **56** 1544 (1986).

[17] P.J. Siemens, Nature **305**, 410 (1983).

[18] L.G. Moretto and G.J. Wozniak, Prog. Part. and Nucl. Phys. **21**, 401 (1988), and references therein.

[19] W.A. Friedman and W.G. Lynch, Phys. Rev. **C28**, 16 (1983).

[20] J. Richert and P. Wagner, Nucl. Phys. **A517**, 399 (1990).

[21] W.A. Friedman, Phys. Rev. Lett. **60**, 2125 (1988).

[22] L.G. Moretto et al., Phys. Rev. Lett. **69**, 1884 (1992).

[23] W. Bauer et al., Phys. Rev. Lett. **69**, 1888 (1992).

[24] D.R. Bowman et al., Phys. Lett. **B282**, 282 (1987).

[25] D.H.E. Gross, Phys. Lett **B203**, 26 (1988).

[26] R. Trockel et al., Phys. Rev. Lett. **59**, 2844 (1987).

[27] Y.D. Kim et al., Phys Rev Lett. **67**, 14 (1991).

[28] Y.D. Kim et al., Phys. Rev. **C45**, 338 (1992).

[29] D. Fox et al., submitted to Phys. Rev. C.

[30] R.T. de Souza et al., Nucl. Instr. Meth. **A295** 109 (1990).

[31] W.L. Kehoe et al., Nucl. Instr. Meth. **311** 258 (1992).

[32] Y.D. Kim et al., Phys. Rev. **C45**, 387 (1992).

[33] S. Pratt, private communication.

[34] The theoretical and experimental correlation functions were normalized in the region $v_{red} > 0.022c$.

[35] For orientation, the distances between the centers of a ^{12}C fragment and the corresponding residues are 8.8 and 9.7 fm for a ^{129}Xe source (projectile) and a ^{193}Bi source (complete fusion), respectively.

[36] The reduced chi-squared values were determined from the ascending portions of the correlation functions, $0.01c \leq v_{red} \leq 0.020$ for high multiplicity events and $0.008c \leq v_{red} \leq 0.015c$ for low multiplicity events.

[37] The maximum angular momentum a ^{129}Xe nucleus can contain with a nonzero fission barrier is 88 $\hbar$.

FIGURES

FIG. 1. Linear density plots of $d^2\sigma/dv_{\|}dv_{\perp}$ for Z=2 (top panels) and Z=6 (bottom panels) fragments. Distributions gated on low (high) charged particle multiplicity, N_C, are shown in the left (right) panels. Regions of red, yellow, green, blue and purple correspond to relative yields of 5, 4, 3, 2 and 1, respectively. The limits of the detector acceptance are indicated by the black lines. The arrows in the left (right) panels indicate the beam (center-of-mass) velocity.

FIG. 2. Experimental correlation functions for $5 \leq Z_1, Z_2 \leq 12$ fragments as a function of the reduced relative velocity, v_{red}. The top (bottom) panel corresponds to high (low) multiplicity events. The solid circles, open circles and open squares correspond to events gated on the indicated ranges of center-of-mass velocity of the two fragments.

FIG. 3. Comparison of experimental correlation functions (solid and open points) with 3-body trajectory calculations (curves). The top panel shows results gated on high multiplicity events, the bottom panel results gated on low multiplicity events for fragments with a center-of-mass velocity >0.3c. The curves correspond to calculations with the indicated source radii, R_S, and mean emission times, τ.

TABLES

TABLE I. Reduced chi-squared values, χ^2/ν, for calculated correlation functions for fragment pairs with V_{CM} >0.3c in low multiplicity collisions.

	R_S (fm)		
τ (fm/c)	8	10	12
500	8.3	14.5	19.4
200	8.8	8.2	4.8
100	76.7	49.5	24.8

TABLE II. Reduced chi-squared values, χ^2/ν, for calculated correlation functions in high multiplicity collisions.

	R_S (fm)		
τ (fm/c)	10	12	14
200	54.3	83.7	106.1
100	7.0	3.5	23.1
50	177.4	32.3	3.8
0	704.5	147.5	26.6

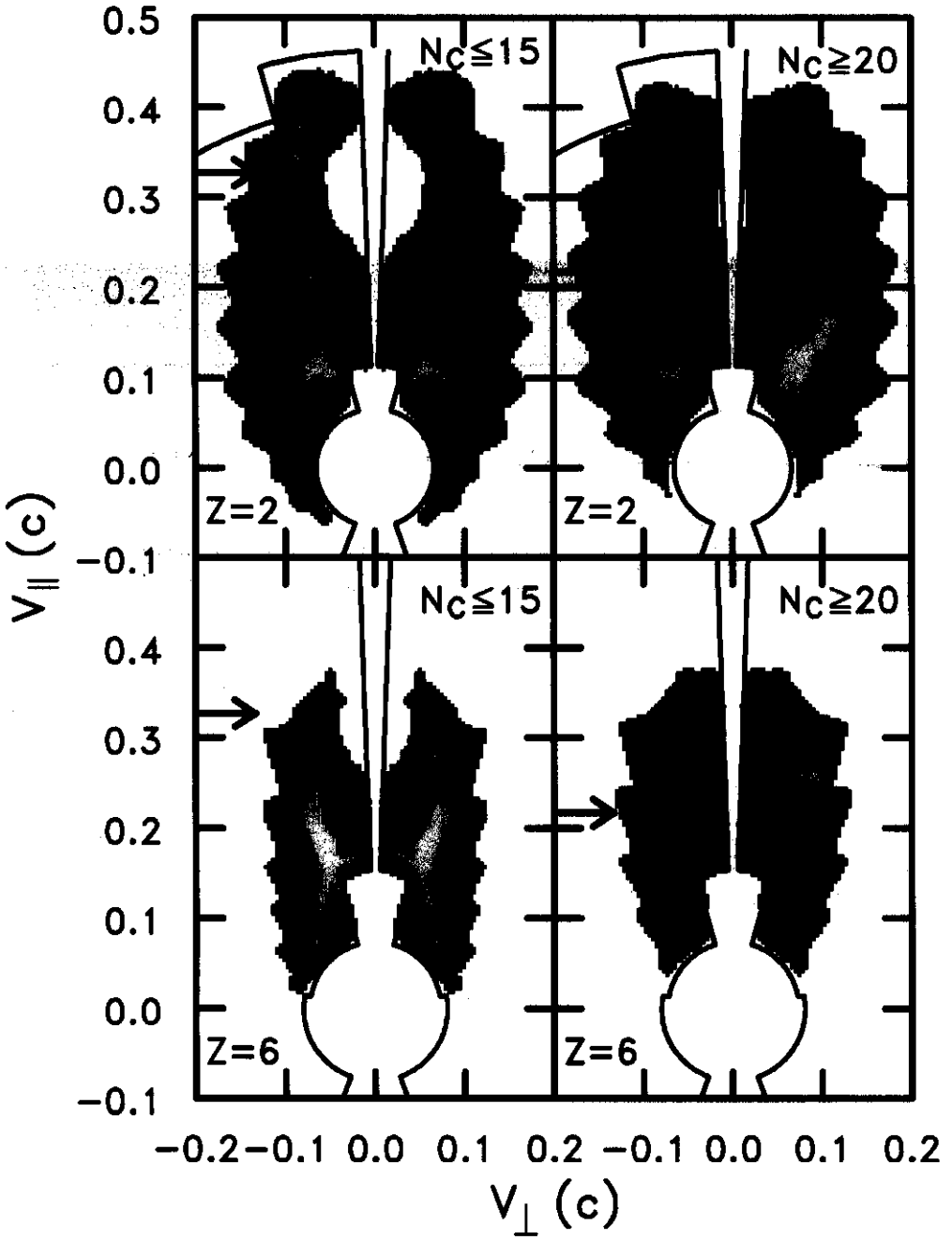
0.5
0.4
0.3
0.2
0.1
0.0
−0.1
$V_{\parallel}$ (c)
Nc≦15
Nc≧20
Z=2
Z=2
Nc≦15
Nc≧20
Z=6
Z=6
−0.2 −0.1 0.0 0.1 0.2 −0.1 0.0 0.1 0.2
$V_{\perp}$ (c)

Fig. 1

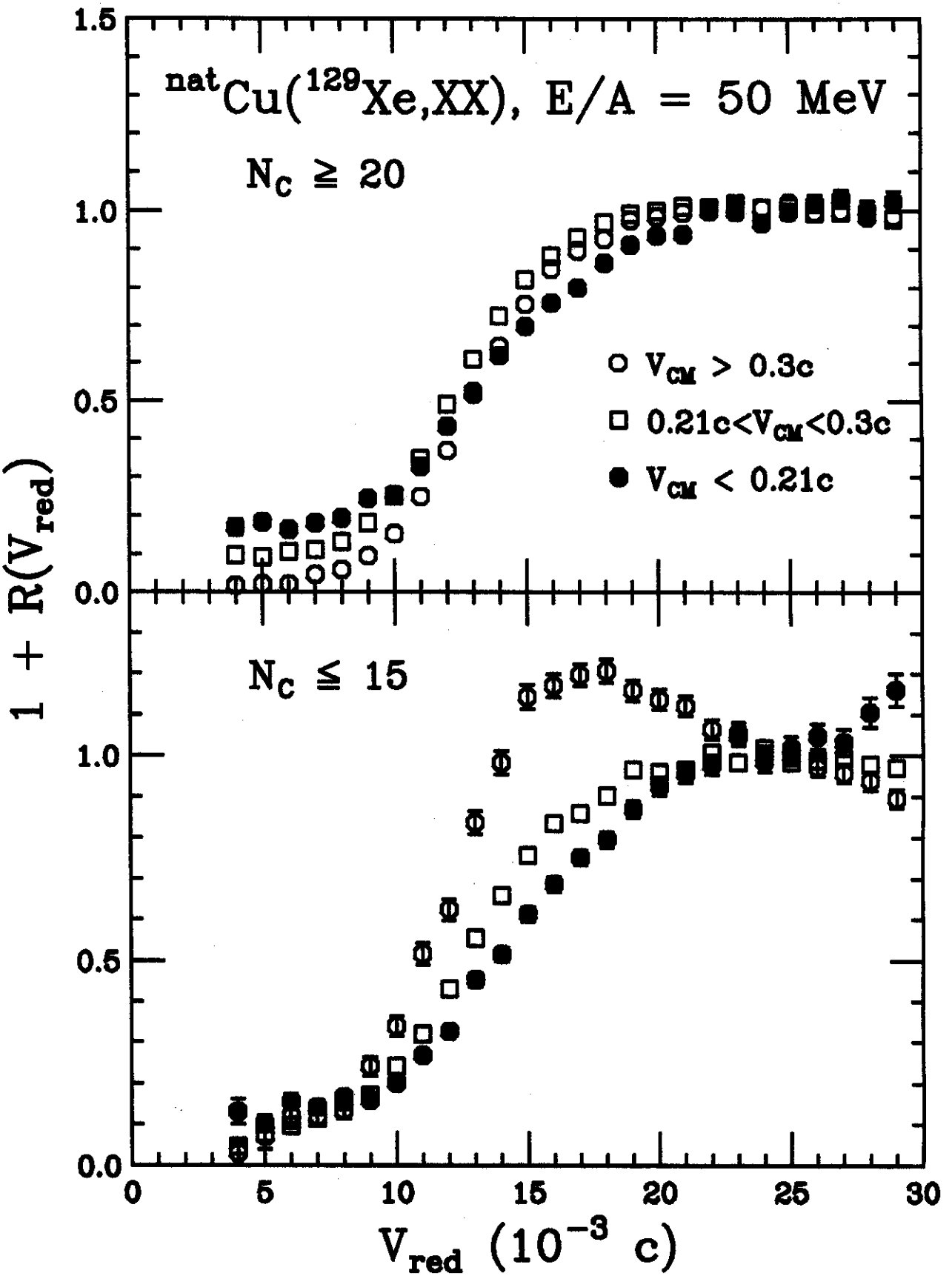
$^{nat}Cu(^{129}Xe,XX)$, E/A = 50 MeV
$N_C \geq 20$
$N_C \leq 15$
$V_{CM} > 0.3c$
$0.21c < V_{CM} < 0.3c$
$V_{CM} < 0.21c$
$1 + R(V_{red})$
V_{red} $(10^{-3}$ c)
0.0
0.5
1.0
1.5
0
5
10
15
20
25
30

FIG 2

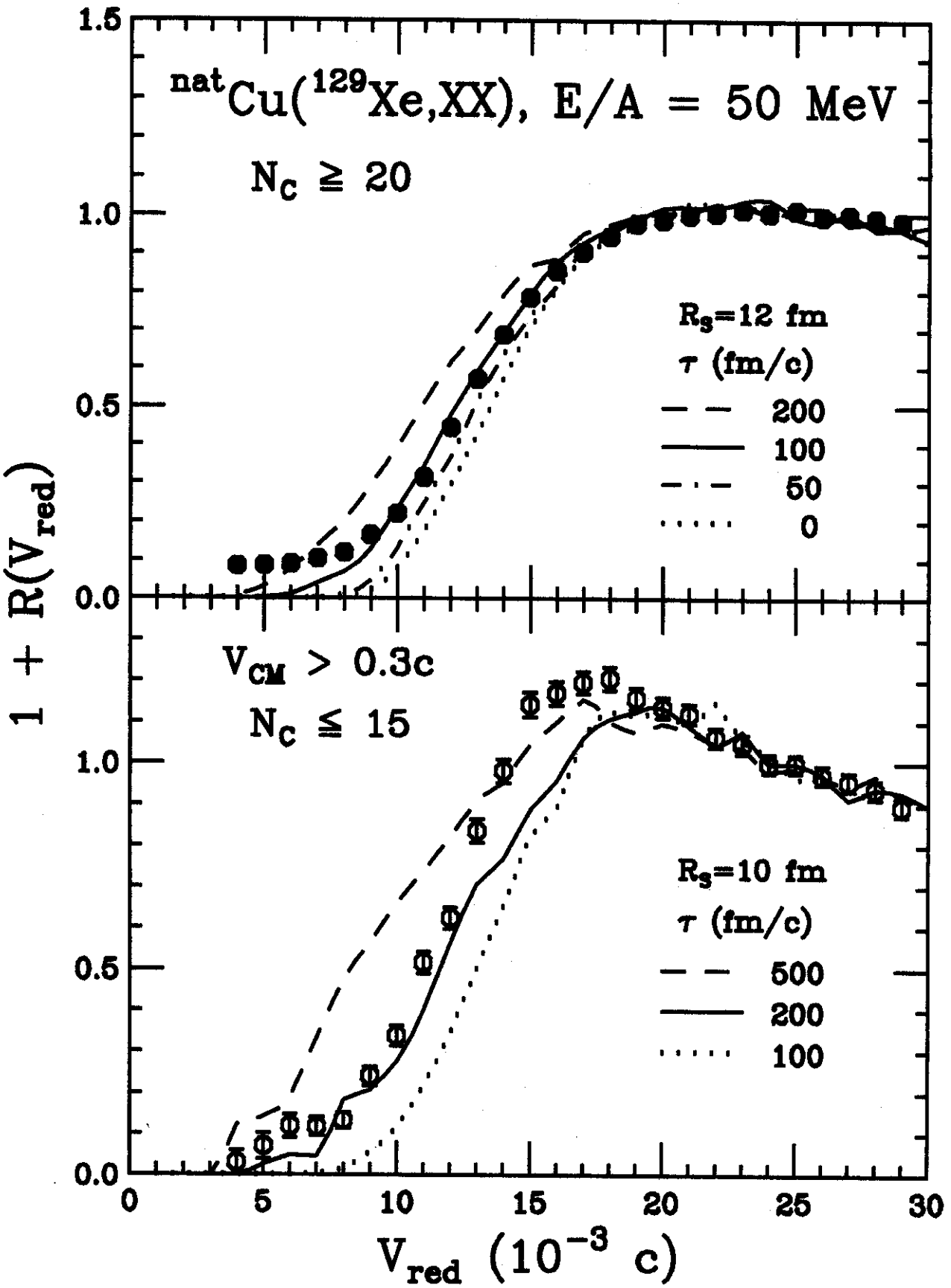
$^{nat}Cu(^{129}Xe,XX)$, E/A = 50 MeV
$N_C \geq 20$
R_s=12 fm
τ (fm/c)
200
100
50
0
$V_{CM} > 0.3c$
$N_C \leq 15$
R_s=10 fm
τ (fm/c)
500
200
100
$1 + R(V_{red})$
V_{red} (10^{-3} c)
0.0
0.5
1.0
1.5
0
5
10
15
20
25
30

FIG 3